Preprints of the 21st IFAC World Congress (Virtual)
Berlin, Germany, July 12-17, 2020

Economic model predictive control for obstacle-aided snake robot locomotion

Evan Müller * **Philipp N. Köhler** * **Kristin Y. Pettersen** **
Frank Allgöwer *

* *Institute for Systems Theory and Automatic Control, University of Stuttgart, Stuttgart, Germany.*
** *Center for Autonomous Marine Operations and Systems, Department of Engineering Cybernetics, Norwegian University of Science and Technology, Trondheim, Norway.*

Abstract: This paper studies the application of economic model predictive control (MPC) to snake robot locomotion. The proposed MPC algorithm integrates the gait pattern creation into the closed loop by maximizing the forward snake velocity. We consider both purely planar locomotion as well as obstacle-aided locomotion. A compliant obstacle-snake contact model is introduced, rendering the interaction dynamics considered in the optimal control problem smooth. We illustrate the efficacy of the scheme by numerical simulations. The emerging gait patterns are undulatory and can make simultaneous use of anisotropic ground friction and obstacles.

Keywords: Model Predictive Control, Mobile robots, Obstacles, Trajectory planning

1. INTRODUCTION

Research on snake robots is inspired by the agile locomotion of biological snakes in a vast range of environments, including cluttered, irregular and constrained spaces as well as under water. Instead of merely avoiding obstacles, snakes incorporate them into their movement by pushing off of well-chosen contact points. Snake robots generally consist of several rigid links connected by powered joints, giving them similar kinematic freedom as biological snakes. Such robots have a broad variety of applications ranging from hazardous search and rescue tasks to sub-sea maintenance with challenging access. A major difficulty in the implementation of snake robots lies in the coordination of the many degrees of freedom to form a gait pattern, which takes advantage of the environment. An overview over previous work on modeling, control and application of snake robots is given in Liljebäck et al. (2012) and Pettersen (2017).

The snake robot coming in contact with and detaching from obstacles introduces discontinuities into the system dynamics, which must be considered when modeling. Principal integration methods for non-smooth systems are the *smoothing* method, *event-driven* method and *timestepping* method (Leine and Nijmeijer, 2004). Transeth et al. (2008) apply timestepping to a snake robot model to accurately simulate the effect of contact forces between links and obstacles as well as ground forces. In Liljebäck et al. (2010, 2011), the hybrid character of the system is used to formulate jump and flow maps triggered at the discrete events of opening or closing contacts.

Existing control architectures for terrestrial snake robots can roughly be divided into three principal approaches: following predefined sine-based waves to create undulatory motion, model-based approaches for gait generation, and central pattern generators (CPG) (Ijspeert and Crespi, 2007). Several control schemes have been introduced specifically for obstacle-aided locomotion. As simple sine-based gaits are too stiff to move through an unstructured array of obstacles, Liljebäck et al. (2011) add a jam resolution scheme. Liljebäck et al. (2014) take contact force measurements into account, "bending" the reference shape such that contact forces face in the desired direction. Travers et al. (2018) combine the sine-based approach with CPG. Predefined waveforms travel down the snake, adapting the waveform locally based on measured joint-torque. The approach is shown to work in real-time in a three-dimensional, cluttered environment without a priori knowledge of the terrain. All these approaches are purely kinematic, omitting the dynamics in the gait pattern creation. Furthermore, obstacles are only taken into account once they have come into contact with the snake. Herein lies an advantage of model predictive control (MPC), which can explicitly consider upcoming obstacles while planning optimal state and input trajectories.

MPC is an optimization-based control method, which repeatedly solves a finite-horizon optimal control problem and applies the first part of the optimal input sequence. While standard MPC aims to stabilize a set point by minimizing a positive definite cost function, economic MPC offers a more general framework permitting the minimization of a general cost (Grüne and Pannek, 2017). So far, little research has been done on the application of MPC to snake robots. In Marafioti et al. (2014), a scalar curve parameter of a predefined gait is controlled via MPC to achieve path following on a planar surface. As the parameters of the sinusoidal gait are chosen offline, this approach is not suited to control a snake surrounded by unstructured obstacles. Nonhoff et al. (2019) propose an economic MPC

scheme for a simplified snake model on a planar surface. Recursive feasibility and performance guarantees such as a minimum velocity are derived. In simulations, the economic MPC scheme is shown to outperform a controller following a sinusoidal reference trajectory.

The work at hand develops an economic MPC control approach for snake robot locomotion in the presence of obstacles. We do not make use of a predefined gait pattern, but rely on the MPC controlling the joint angle accelerations to create the gait in the closed loop. An existing snake model derived from first principles is employed. We introduce a smooth obstacle contact model in order to remove discontinuities from the system dynamics. By considering obstacles in the model, and using a tailored MPC formulation, the emerging gait can exploit these obstacles. A simulation study demonstrates the efficacy of the presented scheme.

This paper is structured as follows: In Section 2, we introduce the employed mathematical model of the snake robot including the compliant contact model. In Section 3 the MPC problem is formulated. Section 4 shows numerical simulation results, followed by concluding remarks in Section 5.

2. MODELING

MPC requires the repeated solution of an optimal control problem. In hybrid systems, it is difficult to find optimal control sequences, as both the combinatorics of the discrete events and continuous dynamics must be considered. This affects the optimization of the snake model as well. Particularly challenging is the fact that we do not know the sequence of contacts between links and obstacles a priori. For this reason, we opt to create a smooth model which captures the relevant properties of snake locomotion, thereby enabling the use of gradient-based optimization. We assume that an accurate representation of the impulsive dynamics is not central to obstacle-aided locomotion.

2.1 Snake model

The snake robot model, briefly presented in the following, is derived in Liljebäck et al. (2012). The two-dimensional snake model consists of N_l identical rigid links, each with the length $2l$, mass m and moment of inertia J. The width of the links is neglected. The external contact and friction forces are assumed to act on the center of each link. This is admissible due to the length of a link being small compared to the snake length. An illustration of the snake robot with the main kinematic and kinetic symbols is given in Figure 1. In the following sections, the optimization of the snake robot is carried out on an input-transformed system. In order to transform the system, the generalized coordinates are split into actuated and unactuated coordinates, q_a and q_u. The actuated degrees of freedom consist of the relative angles between the links $\phi = [\phi_1, \dots, \phi_{N_l-1}]^\mathrm{T}$, whereas the unactuated consist of the angle of the head link θ_{N_l} and the position of the center of mass p_x and p_y

$$q_\mathrm{a} = \phi \in \mathbb{R}^{N_l-1}, \quad q_\mathrm{u} = [\theta_{N_l}, p_x, p_y]^\mathrm{T} \in \mathbb{R}^3.$$

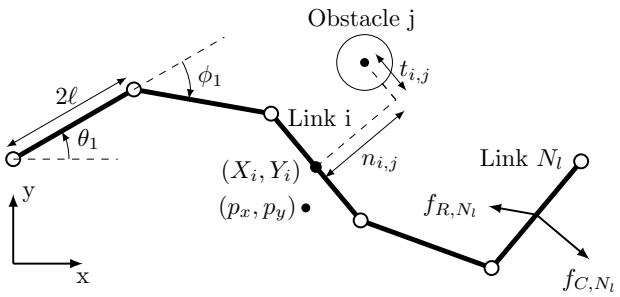

Fig. 1. Schematic representation of the snake robot.

The complete dynamics of the snake robot are given by

$$M_{11}\ddot{q}_\mathrm{a} + M_{12}\ddot{q}_\mathrm{u} + W_1 + G_1\Big[f_\mathrm{R} + f_\mathrm{C}\Big] = \tau \tag{1a}$$

$$M_{21}\ddot{q}_\mathrm{a} + M_{22}\ddot{q}_\mathrm{u} + W_2 + G_2\Big[f_\mathrm{R} + f_\mathrm{C}\Big] = 0_{3\times 1}, \tag{1b}$$

where $f_\mathrm{R} = [f_{\mathrm{R},x}^\mathrm{T}, f_{\mathrm{R},y}^\mathrm{T}]^\mathrm{T} \in \mathbb{R}^{2N_l}$ denotes the ground friction force in the global reference frame acting on each link, $f_\mathrm{C} = [f_{\mathrm{C},x}^\mathrm{T}, f_{\mathrm{C},y}^\mathrm{T}]^\mathrm{T} \in \mathbb{R}^{2N_l}$ the contact force, and $u \in \mathbb{R}^{N_l-1}$ the torque input. For brevity, we refer to Liljebäck et al. (2012) for the definition of the matrices. Applying the input transformation

$$\begin{aligned}\tau = (M_{11} - M_{12}M_{22}^{-1}M_{21})u + W_1 + G_1\big[f_\mathrm{R} + f_\mathrm{C}\big] \\ - M_{12}M_{22}^{-1}(W_2 + G_2\big[f_\mathrm{R} + f_\mathrm{C}\big])\end{aligned} \tag{2}$$

leads to the transformed system

$$\ddot{q}_\mathrm{a} = u \tag{3a}$$

$$\ddot{q}_\mathrm{u} = -M_{22}^{-1}(W_2 + G_2\big[f_\mathrm{R} + f_\mathrm{C}\big]) - M_{22}^{-1}M_{21}u. \tag{3b}$$

The complete state of the system is given by

$$x = [q_\mathrm{a}^\mathrm{T}, q_\mathrm{u}^\mathrm{T}, v_\mathrm{a}^\mathrm{T}, v_\mathrm{u}^\mathrm{T}]^\mathrm{T} \in \mathbb{R}^{2N_l+2}, \tag{4}$$

with $v_\mathrm{a} = \dot{q}_\mathrm{a}$ and $v_\mathrm{u} = \dot{q}_\mathrm{u}$. The position of the center of mass of the individual links in x- and y-direction is denoted by $X = [X_1, ..., X_{N_l}]^\mathrm{T} \in \mathbb{R}^{N_l}$ and $Y = [Y_1, ..., Y_{N_l}]^\mathrm{T} \in \mathbb{R}^{N_l}$, the angle spanned between each link and the x-axis by $\theta = [\theta_1, ..., \theta_{N_l}]^\mathrm{T} \in \mathbb{R}^{N_l}$.

In this work, a viscous model is used for the ground friction force f_R due to its computational simplicity. We apply both isotropic and anisotropic ground friction in this work, only the latter permitting the snake to move forward without obstacles. The ground friction constants c_t and c_n define the friction in the respective normal and tangential link direction. The viscous friction model is described in Liljebäck et al. (2012). While not considered in this paper for the sake of a simpler presentation, the MPC scheme has been shown to work with a smoothed Coulomb friction law too, which represents a more accurate modeling approach.

2.2 Compliant contact model

Aside from the assumption of contact forces acting on the center of the links, we assume that obstacle forces act only in the normal direction of the respective link and that the contacts between links and obstacles are frictionless. Obstacles are considered to be circular and stationary. In a compliant model, the contact force is a continuous function of the distance between the bodies. The forces between all N_l links and the N_o obstacles are considered to act at all times in order to receive a smooth model, but they do

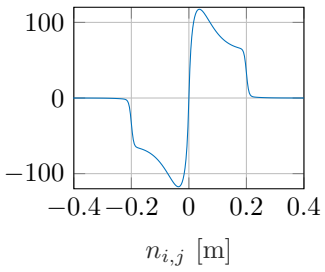

(a) $f_{\mathrm{c},i,j}$ [N], $t_{i,j} = 0$ m

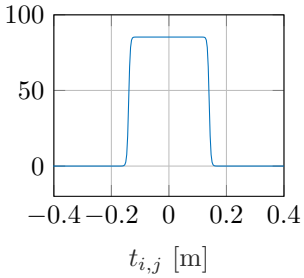

(b) $f_{\mathrm{c},i,j}$ [N], $n_{i,j} = 0.1$ m

Fig. 2. Influence of the normal and tangential obstacle-link distance $n_{i,j}$ and $t_{i,j}$ on the contact force $f_{\mathrm{c},i,j}$.

vary strongly in magnitude. The magnitude and sign of the compliant contact force between link i and obstacle j are described by

$$f_{\mathrm{c},i,j} = \frac{\arctan(an_{i,j})}{(bt_{i,j}/l)^c + 1} \cdot \Big[\frac{d}{(en_{i,j})^g + 1} + \exp(h - 4k|n_{i,j}|)\Big], \tag{5}$$

where $t_{i,j}$ and $n_{i,j}$ are the distance between link i and obstacle j in the normal- and tangential direction, respectively, and a, b, c, d, e, f, g, h, $k > 0$ are constant parameters. This model allows for an intuitive adaptation of the size and stiffness of the obstacles. Making the obstacles very stiff increases the physical accuracy of the model, resembling more closely the non-smooth characteristics of a hard contact. However, this leads to stiffer ODEs. The compliant contact model can be adapted to match requirements on computation time and accuracy. In the following simulations we use $a = 50$, $b = 1$, $c = 50$, $d = 40$, $e = 5$, $g = 16$, $h = 8.5$ and $k = 40$, which approximates obstacles with a radius $r = 0.2$ m. Figure 2 shows how the contact forces depend on $t_{i,j}$ and $n_{i,j}$. Due to a cost term associated with the contact forces in the optimization problem below, it is important for the convergence of the gradient-based optimizer that the contact force in the normal link direction slopes towards the boundary of the obstacle. For this reason, the exponential term is introduced in (5). The forces acting on each link are transformed to the global reference frame by

$$f_{\mathrm{C}} = \begin{bmatrix} -\sin\theta_1 & & 0 \\ & \ddots & \\ 0 & & -\sin\theta_{N_l} \\ \cos\theta_1 & & 0 \\ & \ddots & \\ 0 & & \cos\theta_{N_l} \end{bmatrix} \begin{bmatrix} \sum_{j=1}^{N_o} f_{\mathrm{c},1,j} \\ \vdots \\ \sum_{j=1}^{N_o} f_{\mathrm{c},N_l,j} \end{bmatrix}. \tag{6}$$

The simplifications in the presented contact modeling approach allow for behavior, which cannot occur in the real system. Most notably, the absence of a contact force component in tangential link direction allows link elements to *pierce* obstacles. Only once the link reaches the center of the obstacle does the normal contact force increase steeply, as depicted in Figure 3a. Aside from being unrealistic, this behavior leads to bad convergence of the optimizer, as small changes in the input strongly affect the result. Such behavior can be reduced by introducing a cost on the contact forces. A related effect occurs when a joint passes an obstacle as illustrated in Figure 3b. At this particular position, nearly no contact force is acting on the two links.

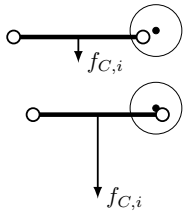

(a) Piercing of an obstacle at two time instances.

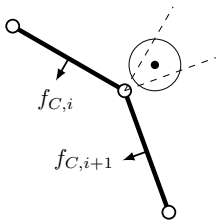

(b) Joint near obstacle.

Fig. 3. Specific problems with compliant contact.

When a cost on the obstacle forces or torques is considered, any movement forward or back is discouraged, which can lead to the snake being "stuck". A possible remedy for this problem lies in a smoother force formulation, as described in the following section.

3. ECONOMIC MPC SCHEME FOR OBSTACLE-AIDED SNAKE ROBOT LOCOMOTION

As a model-based control method, the presented scheme requires a model of the environment surrounding the snake and knowledge of the current state. In a real implementation, this requires state observers and perception. A review of obstacle perception in snake robots is presented by Sanfilippo et al. (2017). The MPC problem for the discrete-time system, which is solved at each time step t, is given by

$$\min_{\mathbf{u}(t)} \sum_{k=0}^{N-1} \ell(x(k|t), u(k|t), \mathbf{O}) + V_{\mathrm{f}}(x(N|t)) \tag{7a}$$

subject to

$$x(k+1|t) = f(x(k|t), u(k|t), \mathbf{O}) \tag{7b}$$
$$x(0|t) = x(t) \tag{7c}$$
$$u(k|t) \in \mathbb{U} \quad \text{for} \quad k = 0, ..., N-1 \tag{7d}$$
$$x(k|t) \in \mathbb{X} \quad \text{for} \quad k = 0, ..., N, \tag{7e}$$

thus optimizing the open-loop trajectory over the prediction horizon N. Hereby, $x(t)$ denotes the system state given in (4). The function f denotes the discrete-time dynamics of the system including interaction with the set of obstacles $\mathbf{O} = \{\mathbf{O}_1, ..., \mathbf{O}_{N_o}\} \in \mathbb{R}^{3N_o}$ defining the position and radius of each obstacle, thus f is a discretized version of (3). In this formulation, the input u represents the joint angle acceleration. The predicted time series at time t are denoted as $\mathbf{u}(t) = \{u(0|t), ..., u(N-1|t)\}$ and $\mathbf{x}(t) = \{x(0|t), ..., x(N|t)\}$. The sets $\mathbb{U}$ and $\mathbb{X}$ represent state and input constraints, $\ell : \mathbb{X} \times \mathbb{U} \times \mathbb{R}^{3N_l} \to \mathbb{R}$ an arbitrary stage cost and $V_{\mathrm{f}} : \mathbb{X} \to \mathbb{R}$ a terminal cost. At each time t, the first element of the optimal open-loop input sequence is applied to the system, i.e., $u(t) = u(0|t)$. Our overall aim is to maximize the velocity of the snake in the x-axis direction. This aim is implemented by a proper choice of the stage cost function and a terminal cost on the advancement of the snake over the prediction horizon N. The choice of measure for this advancement is discussed in the following section.

The snake robot has mechanical restrictions, which are incorporated through constraints. In particular the joint angle is limited by design, hence,

$$\mathbb{X} = \{x(t) \in \mathbb{R}^{2N_l+2} | \phi_i(t) \in [-\phi_{\max}, \phi_{\max}], i = 1, ..., N_l - 1\}. \tag{8}$$

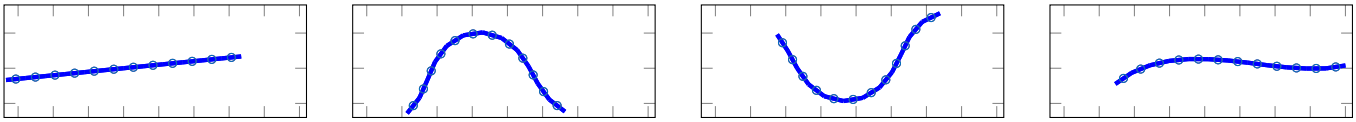

(a) $t = 0$ s (b) $t = 5.2$ s (c) $t = 10.3$ s (d) $t = 15.5$ s

Fig. 4. Open-loop trajectory with $T = 15.5$, $N = 105$ maximizing the position of the head link N_l with $c_\mathrm{t} = 1$, $c_\mathrm{n} = 2$.

We introduce box constraints on the input $u(t)$, representing a purely kinematical limit of the joint angle acceleration

$$\mathbb{U} = \{u(t) \in \mathbb{R}^{N_l-1} | u_i(t) \in [-u_{\max}, u_{\max}], i = 1, ..., N_l-1\}. \tag{9}$$

Ideally, the mechanical torque constraints of the joints are taken into account directly by considering the constraint $-\tau_{\max} \leq \tau \leq \tau_{\max}$. Due to the complexity of (2), this greatly increases the difficulty of the optimization problem. We were not able to achieve convergence of the optimization problem under consideration of this constraint. Completely omitting the torque limits of the snake robot may, however, lead to undesirable results. In specific configurations, the high torques can lead to links passing through compliant obstacles, thereby generating very large contact forces. As a way of preventing this unrealistic mechanism, we incorporated into the cost soft constraints on either the contact forces or on the joint reaction torques, given by

$$\ell_\mathrm{f}(x, u, \mathbf{O}) = \sum_{j=1}^{N_o} \sum_{i=1}^{N_l} \hat{f}^2_{\mathrm{c},i,j}, \tag{10}$$

$$\ell_\mathrm{t}(x, u, \mathbf{O}) = \sum_{i=1}^{N_l} \Big((M_{11} - M_{12}M_{22}^{-1}M_{21})u + W_1 + G_1\hat{f}_\mathrm{C} - M_{12}M_{22}^{-1}(W_2 + G_2\hat{f}_\mathrm{C}) \Big)^2, \tag{11}$$

respectively. In the aforementioned soft constraints, the force formulation $\hat{f}_{\mathrm{c},i,j}$ is a conservative approximation to the contact force $f_{\mathrm{c},i,j}$ used in the system dynamics (3). This decreases the computational effort and can prevent the snake from getting "stuck" as described in the previous section and depicted in Figure 3b. $\hat{f}_{c,i,j}$ is computed analogous to $f_{c,i,j}$ via (5), but employs an alternative set of parameters. In the following simulations, we use $\hat{a} = 50$, $\hat{b} = 0.7$, $\hat{c} = 10$, $\hat{d} = 40$, $\hat{e} = 5$, $\hat{g} = 16$, $\hat{h} = 8.5$ and $\hat{k} = 40$.

Another mechanical restriction is that two joints cannot overlap. We do not model link-link-contact, but can conservatively prevent such contact by constraining the heading angle of each link via $-\frac{\pi}{2} \leq \theta_i \leq \frac{\pi}{2}$ for $i = 1, ..., N_l$. While this constraint limits the possible gait patterns, it is viable as it assumes that links at no point face away from the targeted direction during efficient forward locomotion. As this requirement only serves as a guidance trying to avoid a "bunching up" of the snake, it can be replaced by a soft constraint introduced into the cost by the term

$$\ell_\theta(x, u) = \sum_{i=1}^{N_l} \Big(\max(0,\ |\theta_i| - \frac{\pi}{2}) \Big)^2. \tag{12}$$

Having introduced hard constraints only on the joint angles ϕ, and the input being $u = \ddot{\phi}$, recursive feasibility of the MPC scheme can be verified straightforwardly.

4. SIMULATION STUDY

In this section the efficacy of the proposed MPC scheme is demonstrated through numerical simulations. The MPC algorithm was implemented using the optimization tool CasADi (Andersson et al., 2018). Hereby, the NLP solver IPOPT is used, running with the linear solver MUMPS. The optimization problem is discretized via the multiple-shooting method. The time integration of the continuous time dynamics of the system is carried out with the classical Runge-Kutta method. At each sampling time, the previous solution is taken to warm start the solver. The simulated snake robot consists of $N_l = 12$ equal links with a mass of $m = 1$ kg, link length $2l = 0.28$ m and moment of inertia $J = 0.016$ kg m^2. The snake is initialized such that it is in an equilibrium state with the obstacle contact forces. The constraint sets are given by $\phi_{\max} = 0.45\pi$ and $u_{\max} = 0.15$. The parameters appearing in the following cost functionals are tuned towards the desired performance.

4.1 Planar Locomotion

Snakes can move on planar surfaces, if they exhibit anisotropic friction behavior between the links and the ground surface. Although the main advantage of snake robots over wheeled and legged robots is their mobility in rough terrain, the robot also needs to be able to traverse planar surfaces. Moreover, the planar case serves as a starting point to the locomotion problem and represents the special case $\mathbf{O} = \{\}$ in the problem formulation.

At first, we regard the open-loop behavior of the snake, i.e., the solution of the optimization problem posed in (7a). It is typical for economic MPC without terminal constraints to show the so called *turnpike* behavior. This means that open-loop trajectories spend most of the finite prediction horizon in a neighborhood of the periodic or steady-state infinite-horizon optimal operating behavior. Towards the end of the open-loop prediction, a *leaving arc* deviates from this optimal operating behavior. The number of time steps consumed by the leaving arc is independent of the prediction horizon (Angeli and Müller, 2019).

For the case of the snake robot on a planar surface, the optimal infinite-horizon operating behavior is a periodic orbit. An example of an open-loop trajectory with $N = 105$, $T = 15.5$ s, $c_\mathrm{t} = 1$, $c_\mathrm{n} = 2$, and considering minimization of the following cost functional in (7a)

$$\sum_{k=0}^{N-1} 10\ell_\theta(x(k|t), u(k|t)) - 6X_{N_l}(N|t), \tag{13}$$

is shown in Figure 4. After a transient period, the snake enters a periodic orbit resembling an undulation pattern. At the end of the prediction, the trajectory leaves the

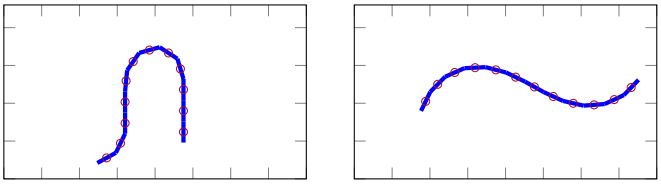

(a) Center of mass. (b) Sinusoidal terminal cost.

Fig. 5. Snake state at the end of prediction horizon with different terminal costs.

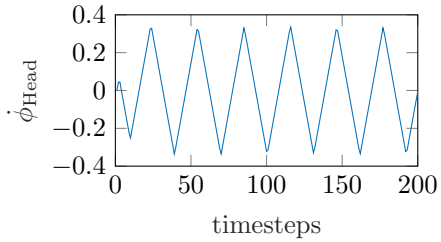

Fig. 6. Angular velocity of joint $N_l - 1$ (head joint).

periodic orbit. The occurring leaving arc is largely influenced by the terminal cost $V_{\text{f}}(x(N|t))$. In the example shown in Figure 4, the terminal cost is the position of the head link along the x-axis. The snake achieves a short-term advantage by fully stretching out. Alternatively, the terminal cost could be chosen as the position of the center of mass p_x. Under these conditions, the final state of the open-loop trajectory is of the shape shown in Figure 5a, where the snake takes on a U-shape. Out of the possible terminal costs, we consider maximizing the head link position to be most desirable, as the leaving arc is limited to fully stretching out and it does not rely on additional constraints to prevent undesired terminal states. Overall, the final state of the open loop is not beneficial to the advancement beyond the prediction horizon. Ideally, we aim to avoid the influence of the leaving arc in the closed loop, which requires a sufficiently long prediction horizon.

Applying MPC with cost functional (13) to the nominal snake model (3) results in the closed-loop system reaching and remaining on a periodic orbit after a short transition period. Figure 6 shows the velocity of the head joint angle over time to form a triangle wave in the closed loop, clearly differing from the sinusoidal velocity commonly associated with lateral undulation. A similar velocity pattern was observed in Nonhoff et al. (2019). The MPC scheme adapts the gait pattern according to the ground friction conditions. For the friction coefficients $c_{\text{t}} = 1$ and $c_{\text{n}} = 2$, the scheme achieves an average velocity of $\bar{v} = 0.068$ m/s with a period length of $P = 2.45$ s, while $c_{\text{t}} = 1$ and $c_{\text{n}} = 20$ leads to $\bar{v} = 0.32$ m/s with $P = 1.87$ s.

It is known from literature that sinusoidal joint inputs create adequate locomotion (Liljebäck et al., 2012). In an attempt to reduce the leaving arc, we introduce an additional terminal cost which should approximate the infinite horizon cost by penalizing deviations from the closest sinusoidal reference joint angles and velocities in the final state. We define the terminal costs V_θ and $V_{v,\theta}$ as

$$V_\theta(\mathbf{x}(t), t) = \min_{\theta_0} ||\theta(N|t) - \theta_{\text{ref}}(\theta_0)||$$
$$V_{v,\theta}(\mathbf{x}(t), t) = \min_{\theta_0} ||v_\theta(N|t) - v_{\theta_{\text{ref}}}(\theta_0)||,$$

where θ_{ref} is dependent on the amplitudes w_1, w_2, the scalar optimization variable θ_0 represents the overall phase shift, and θ_δ the desired phase shift between the joints.

$$\theta_{\text{ref}} = w_1 \begin{bmatrix} \sin(1\theta_\delta + \theta_0) \\ \vdots \\ \sin(N_l\theta_\delta + \theta_0) \end{bmatrix}, v_{\phi,\text{ref}} = w_2 \begin{bmatrix} \cos(1\theta_\delta + \theta_0) \\ \vdots \\ \cos(N_l\theta_\delta + \theta_0) \end{bmatrix}.$$

The cost functional in (7a) is then given as

$$\min_{\theta_0} \sum_{k=0}^{N-1} 10\ell_\theta(x(k|t), u(k|t)) - 6X_{N_l}(N|t) + 10||\theta(N|t) - \theta_{\text{ref}}(\theta_0)|| + 10||v_\theta(N|t) - v_{\theta_{\text{ref}}}(\theta_0)||.$$

We set $\phi_\delta = 0.4$, $w_1 = 0.4$ and $w_2 = 0.6$. The final state of the open-loop prediction is depicted in Figure 5b. This approach allows to adapt the proposed MPC scheme to computational restrictions, following more closely the predefined sinusoidal reference trajectory for small prediction horizons or allowing more flexibility for longer prediction horizons.

4.2 Obstacle-Aided Locomotion

As the MPC scheme is able to create useful gaits in the closed loop in the planar case, we proceed by including obstacles in the dynamics. Obstacle-snake interaction is modeled by the compliant contact force with the parameters listed in Section 2.2. At first, we assume isotropic ground friction with $c_{\text{t}} = c_{\text{n}} = 20$, such that the snake must fully rely on obstacles to move forward. We set $N = 55$, $T = 7.5$ s and employ in (7a) the composed cost functional

$$\sum_{k=0}^{N-1} 3000\ell_\theta(x(k|t), (k|t)) + 0.002\ell_{\text{t}}(x(k|t), (k|t), \mathbf{O}) - 100X_{N_l}(N|t),$$

thus penalizing high, unrealistic joint torques via the soft constraint cost given in (11). Figure 7 shows snapshots of the resulting MPC closed-loop behavior of the snake. The created gait resembles lateral undulation and makes efficient use of the obstacles in the intended fashion. Figure 8 shows the behavior with the cost functional

$$\sum_{k=0}^{N-1} 3000\ell_\theta(x(k|t), (k|t)) + 0.0004\ell_{\text{f}}(x(k|t), u(k|t), \mathbf{O}) - 100X_{N_l}(N|t),$$

which penalizes high contact forces instead of joint torques. This case results in slightly different motion. Specifically, Figures 7-8 show that applying a torque cost favors serpentine motion, while the force cost promotes a push- and pull behavior. The choice between these two approaches can thus be made depending on the desired behavior. Numerically, the simpler force cost has shown to be more robust, in particular when many obstacles are present. The cost on joint torques can, on the other hand, more closely approximate a constraint on the torque, if this is a limiting factor.

While the above simulation illustrated the case with isotropic ground friction, it is realistic that locomotion

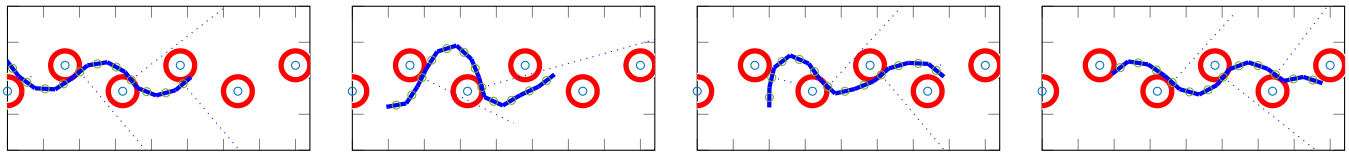

(a) $t = 2.7$ s (b) $t = 5.4$ s (c) $t = 8.2$ s (d) $t = 10.9$ s

Fig. 7. Closed-loop behavior with $T = 7.5$ s, $N = 55$, using cost on joint torque, isotropic friction.

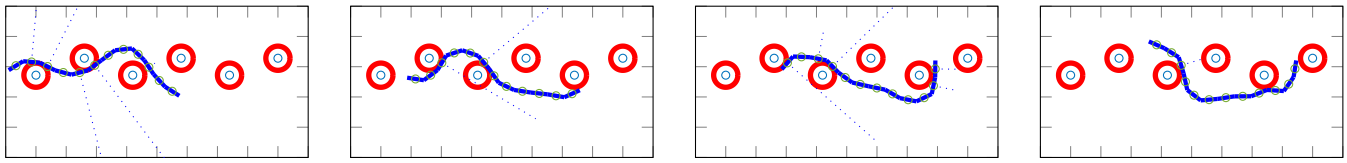

(a) $t = 2.7$ s (b) $t = 9.5$ s (c) $t = 16.4$ s (d) $t = 23.9$ s

Fig. 8. Closed-loop behavior with $T = 7.5$ s, $N = 55$, using cost on contact force, isotropic friction.

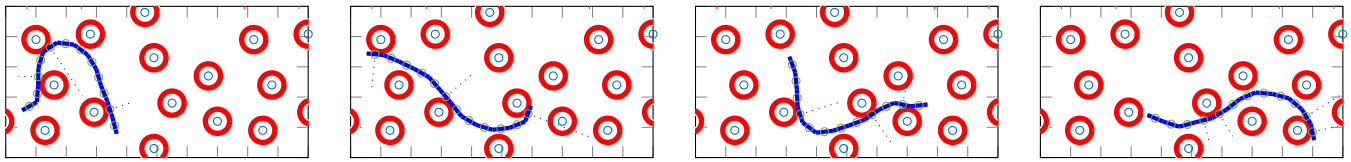

(a) $t = 8.2$ s (b) $t = 13.6$ s (c) $t = 19.1$ s (d) $t = 24.5$ s

Fig. 9. Closed-loop behavior with $T = 7.5$ s, $N = 55$, using cost on contact force, anisotropic friction.

is generated both by anisotropic ground friction and by obstacles. Figure 9 shows the closed loop result of a simulation under these conditions with the same controller configuration as in the previous case. We prescribe an arbitrary unstructured array of obstacles and the friction coefficients $c_\mathrm{n} = 20$ and $c_\mathrm{t} = 7$. The emerging gait pattern clearly makes use of both locomotion methods, passing by obstacles in a fluent manner.

The computation of each optimal input in the presented simulations takes between 5 and 200 seconds on a desktop computer running C code on a virtual machine. Clearly, this by far exceeds the simulation step time, thus rendering a real-time use of this implementation impossible. It should be noted that no effort was made specifically to reduce computation time, the the runtimes of this experimental implementation are only noted for completeness.

4.3 MPC of a hybrid snake model

In the previous simulations, the optimization model employed in the model predictive control formulation (7a) is chosen to be identical to the controlled snake model. It is of interest to assess whether the compliant contact model is able to approximate the hybrid dynamics of the system sufficiently well and, in turn, whether MPC based on the smooth optimization model is able to produce useful control inputs for the hybrid model. As a proof of concept, a closed-loop simulation of a hybrid model controlled by the MPC scheme based on the compliant contact model is carried out. The hybrid model used in the following simulations is based on Liljebäck et al. (2010). It uses the same snake kinematics as the model shown in Figure 1, and the same generalized coordinates $q = [q_\mathrm{a}^\mathrm{T}, q_\mathrm{u}^\mathrm{T}]^\mathrm{T}$. The main difference is that in the hybrid model, impacts between links and obstacles are assumed to be inelastic, whereas they are fully elastic in the compliant contact model. Unlike the compliant contact model, the hybrid model shows no distance effects, as the links are only subject to the obstacle force once contact is established. The ground friction in the two models are identical; in the following we assume anisotropic viscous ground friction with the friction coefficients $c_\mathrm{n} = 20$ and $c_\mathrm{t} = 10$. The simulation step times are set to 5×10^{-5} s. At every time step, possible impacts or detachments are tested for. Depending on the detected event, the respective jump map or flow map is triggered. The flow map, describing the continuous dynamics and integrated using a Runge-Kutta method, is given by

$$M_{11}\ddot{q}_\mathrm{a} + M_{12}\ddot{q}_\mathrm{u} + W_1 + G_1 f_\mathrm{R} = \tau + \bar{C}_1^\mathrm{T}\lambda \tag{14a}$$

$$M_{21}\ddot{q}_\mathrm{a} + M_{22}\ddot{q}_\mathrm{u} + W_2 + G_2 f_\mathrm{R} = \bar{C}_2^\mathrm{T}\lambda, \tag{14b}$$

where the matrices $\bar{C}_1$ and $\bar{C}_2$ give the normal link direction for those links which are in contact with an obstacle at a given time. For brevity, we refer to Liljebäck et al. (2010) for the definition of the matrices. The vector of Lagrange multipliers $\lambda \in \mathbb{R}^{2N_l}$ gives the magnitude of the constraint forces. The constraint condition on acceleration level is given by

$$\dot{\bar{C}}\dot{q} + \bar{C}\ddot{q} \geq 0, \qquad \lambda \geq 0, \qquad \lambda^\mathrm{T}(\dot{\bar{C}}\dot{q} + \bar{C}\ddot{q}) = 0. \tag{15}$$

The MPC scheme computes a kinematic input containing the joint angle accelerations. In order to apply these to the hybrid model, an input transformation is carried out, corresponding to the one applied to the compliant contact model in (2).

$$\begin{aligned}\tau = (M_{11} - M_{12}M_{22}^{-1}M_{21})u + W_1 + G_1 f_\mathrm{R} \\ - M_{12}M_{22}^{-1}(W_2 + G_2 f_\mathrm{R} - \bar{C}_2^\mathrm{T}\lambda) - \bar{C}_1^\mathrm{T}\lambda.\end{aligned} \tag{16}$$

The dynamics of the system can now be rewritten as

$$\ddot{q}_\mathrm{a} = u \tag{17a}$$

$$\ddot{q}_\mathrm{u} = -M_{22}^{-1}\left(W_2 + G_2 f_\mathrm{R} - \bar{C}_2^\mathrm{T}\lambda\right) - M_{22}^{-1}M_{21}\ddot{q}_\mathrm{a}. \tag{17b}$$

Into the constraint condition (15) we insert

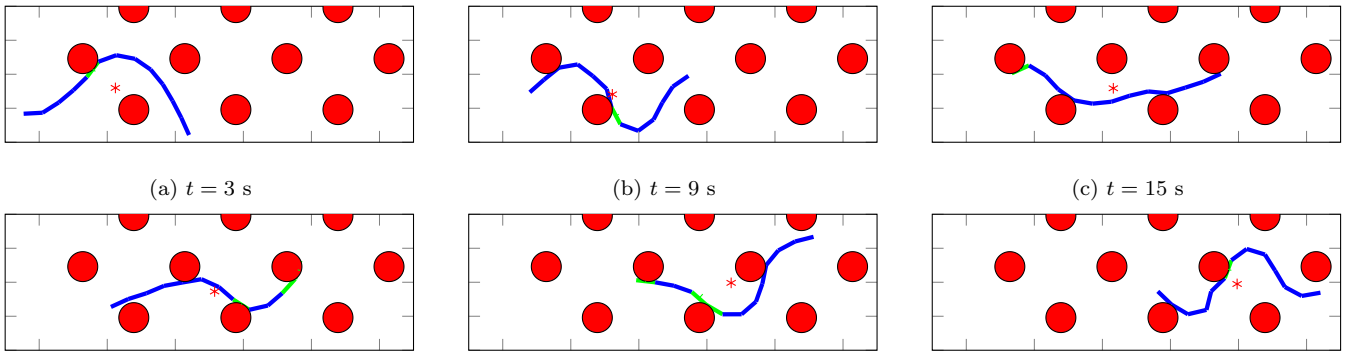

(a) $t = 3$ s (b) $t = 9$ s (c) $t = 15$ s

(d) $t = 21$ s (e) $t = 27$ s (f) $t = 24.5$ s

Fig. 10. Hybrid Plant, closed-loop behavior with $T = 7.5$ s, $N = 55$, using cost on contact force, anisotropic friction. Green links are in contact with an obstacle. The red asterisk depicts the snake's center of mass.

$$\dot{\bar{C}}\dot{q}+\bar{C}\ddot{q} = \bar{C}M^{-1}\Big[-W-Gf_{\mathrm{R}}+B\Big((M_{11}-M_{12}M_{22}^{-1}M_{21})u + W_1 + G_1 f_{\mathrm{R}} - M_{12}M_{22}^{-1}(W_2+G_2 f_{\mathrm{R}})\Big)\Big] + \dot{\bar{C}}\dot{q} + \bar{C}M^{-1}\Big[\bar{C}^{\mathrm{T}} + B\Big(-\bar{C}_1^{\mathrm{T}} + M_{12}M_{22}^{-1}\bar{C}_2^{\mathrm{T}}\Big)\Big]\lambda.$$

The resulting linear complementarity problem (LCP) is solved via the Lemke algorithm (see Liljebäck et al. (2010)). Whenever a contact is closed, the jump map is called. Thereby, we assume that the generalized coordinates before and after impact are identical, i.e. $q^+ = q^-$, and that the joint angle velocities are not affected by impact, i.e. $\dot{q}_{\mathrm{a}}^+ = \dot{q}_{\mathrm{a}}^-$. Introducing the vector of impulsive forces as $\Lambda \in \mathbb{R}^{2N_l}$, the discontinuous dynamics are

$$\dot{q}_{\mathrm{u}}^+ = \dot{q}_{\mathrm{u}}^- + [M_{12}^{\mathrm{T}}, M_{22}^{\mathrm{T}}]^{-\mathrm{T}}\bar{C}^{\mathrm{T}}\Lambda. \tag{18}$$

The complementary conditions, again resulting in an LCP, are given by

$$\bar{C}\dot{q}^+ \geq 0, \qquad \Lambda \geq 0, \qquad \Lambda^{\mathrm{T}}\bar{C}\dot{q}^+ = 0, \tag{19}$$

with

$$\bar{C}\dot{q}^+ = \bar{C}\dot{q}^- + \bar{C}_2[M_{12}^{\mathrm{T}}, M_{22}^{\mathrm{T}}]^{-\mathrm{T}}\bar{C}^{\mathrm{T}}\Lambda. \tag{20}$$

Figure 10 shows snapshots of the hybrid snake model resulting from MPC closed-loop control. A similar behavior as in the simulations of Sections 4.1 and 4.2 shown in Figure 9, where MPC was applied to the nominal compliant snake model, can be observed. We conclude that under the given conditions, the chosen compliant contact model is a valid choice in order to generate, by means of MPC, control inputs for a realistic hybrid snake model moving in obstacle-cluttered environments.

5. CONCLUSION

This work presented an economic MPC scheme for snake robots, which offers a holistic control approach combining gait creation and actuation in the closed loop. A simulation study was performed, demonstrating the ability of the scheme to consider both ground friction and obstacles in the gait creation. Due to the predictive nature of an MPC controller, obstacles are considered before having come into contact with the snake. The robustness of the scheme with respect to model uncertainties remains to be studied in detail. In order to implement the controller on a real system, future work on an efficient numerical implementation and on the perception of the environment is required.

REFERENCES

Andersson, J.A.E., Gillis, J., Horn, G., Rawlings, J.B., and Diehl, M. (2018). Casadi – a software framework for nonlinear optimization and optimal control. *Mathematical Programming Computation*, 11(1), 1–36.

Angeli, D. and Müller, M.A. (2019). *Economic Model Predictive Control: Some Design Tools and Analysis Techniques*, 145–167. Springer International Publishing, Cham.

Grüne, L. and Pannek, J. (2017). *Nonlinear Model Predictive Control*. Communications and Control Engineering. Springer, Berlin.

Ijspeert, A.J. and Crespi, A. (2007). Online trajectory generation in an amphibious snake robot using a lamprey-like central pattern generator model. In *Proc. IEEE Int. Conf. on Robotics and Automation*, 262–268.

Leine, R.I. and Nijmeijer, H. (eds.) (2004). *Dynamics and bifurcations of non-smooth mechanical systems*. Springer, Berlin.

Liljebäck, P., Pettersen, K.Y., Stavdahl, Ø., and Gravdahl, J. (2010). Hybrid modelling and control of obstacle-aided snake robot locomotion. *IEEE Transactions on Robotics*, 26(5), 781 – 799.

Liljebäck, P., Pettersen, K.Y., Stavdahl, Ø., and Gravdahl, J. (2012). *Snake Robots: Modelling, Mechatronics, and Control*. Advances in Industrial Control. Springer, London.

Liljebäck, P., Pettersen, K.Y., Stavdahl, Ø., and Gravdahl, J. (2014). Compliant control of the body shape of snake robots. In *Proc. IEEE Int. Conf. on Robotics and Automation*, 4548–4555.

Liljebäck, P., Pettersen, K.Y., Stavdahl, Ø., and Gravdahl, J.T. (2011). Experimental investigation of obstacle-aided locomotion with a snake robot. *IEEE Transactions on Robotics*, 27(4), 792–800.

Marafioti, G., Liljebäck, P., and Transeth, A.A. (2014). A study of nonlinear model predictive control (NMPC) for snake robot path following. In *Proc. IEEE Int. Conf. on Robotics and Biomimetics*, 568–573.

Nonhoff, M., Köhler, P.N., Kohl, A.M., Pettersen, K.Y., and Allgöwer, F. (2019). Economic model predictive control for snake robot locomotion. In *Proc. 58th IEEE Conf. on Decision and Control*, accepted. URL `https://arxiv.org/abs/1909.00795`.

Pettersen, K.Y. (2017). Snake robots. *Annual Reviews in Control*, 44, 19 – 44.

Sanfilippo, F., Azpiazu, J., Marafioti, G., Transeth, A., Stavdahl, Ø., and Liljebäck, P. (2017). Perception-driven obstacle-aided locomotion for snake robots. *Applied Sciences*, 7, 336.

Transeth, A., Leine, R., Glocker, C., Pettersen, K.Y., and Liljebäck, P. (2008). Snake robot obstacle-aided locomotion: Modeling, simulations, and experiments. *IEEE Transactions on Robotics*, 24, 88 – 104.

Travers, M.J., Whitman, J., and Choset, H. (2018). Shape-based coordination in locomotion control. *I. J. Robotics Res.*, 37.